Global Cooling During the Eocene-Oligocene Climate Transition

Zhonghui Liu, *et al.*

Science **323**, 1187 (2009);
DOI: 10.1126/science.1166368

12. D. Hsieh *et al.*, *Nature* **452**, 970 (2008).
13. S.-C. Zhang, T. H. Hansson, S. Kivelson, *Phys. Rev. Lett.* **62**, 82 (1989).
14. F. Wilczek, *Phys. Rev. Lett.* **58**, 1799 (1987).
15. J. D. Jackson, *Classical Electrodynamics* (Wiley, New York, 1999).
16. E. Witten, *Phys. Lett. B* **86**, 283 (1979).
17. See supporting material on *Science* Online.
18. O. Madelung, U. Rössler, M. Schulz, in *Landolt-Börnstein, Substance/Property Index, Semiconductors, Non-Tetrahedrally Bonded Elements and Binary Compounds I, Subvolume III/17E-17F-41C* (Springer, Berlin, 1998), pp. 1–11.
19. C. Castelnovo, R. Moessner, S. L. Sondhi, *Nature* **451**, 42 (2008).
20. J. Leinaas, J. Myrheim, *Nuovo Cim. B* **37**, 1 (1977).
21. F. Wilczek, *Phys. Rev. Lett.* **49**, 957 (1982).
22. R. Jackiw, C. Rebbi, *Phys. Rev. Lett.* **36**, 1116 (1976).
23. P. Hasenfratz, G. 't Hooft, *Phys. Rev. Lett.* **36**, 1119 (1976).
24. E. Fradkin, S. Kivelson, *Nucl. Phys. B* **474**, 543 (1996).
25. C. Chamon *et al.*, *Phys. Rev. Lett.* **100**, 110405 (2008).
26. We thank O. M. Auslaender, T. L. Hughes, S. Kivelson, and L. Luan for insightful discussions. This work is supported by the U.S. Department of Energy, Office of Basic Energy Sciences under contract DE-AC03-76SF00515.

Supporting Online Material

www.sciencemag.org/cgi/content/full/1167747/DC1
SOM Text
Figs. S1 to S5
References

27 October 2008; accepted 16 January 2009
Published online 29 January 2009;
10.1126/science.1167747
Include this information when citing this paper.

Global Cooling During the Eocene-Oligocene Climate Transition

Zhonghui Liu,[1,2]* Mark Pagani,[1]* David Zinniker,[1] Robert DeConto,[3] Matthew Huber,[4] Henk Brinkhuis,[5] Sunita R. Shah,[6] R. Mark Leckie,[3] Ann Pearson[6]

About 34 million years ago, Earth's climate shifted from a relatively ice-free world to one with glacial conditions on Antarctica characterized by substantial ice sheets. How Earth's temperature changed during this climate transition remains poorly understood, and evidence for Northern Hemisphere polar ice is controversial. Here, we report proxy records of sea surface temperatures from multiple ocean localities and show that the high-latitude temperature decrease was substantial and heterogeneous. High-latitude (45 degrees to 70 degrees in both hemispheres) temperatures before the climate transition were ~20°C and cooled an average of ~5°C. Our results, combined with ocean and ice-sheet model simulations and benthic oxygen isotope records, indicate that Northern Hemisphere glaciation was not required to accommodate the magnitude of continental ice growth during this time.

The abrupt shift to glacial conditions near the Eocene-Oligocene (E-O) boundary ~33.7 million years ago (Ma) is characterized by a ~+1.5 per mil (‰) change in oxygen isotopic ($\delta^{18}O$) values of benthic foraminifera (*1*–*3*) in ~300,000 years, which is indicative of continential ice accumulation and high-latitude cooling, and an ~1-km deepening of the global calcite compensation depth (CCD) (*2*). Proposed causes for this fundamental change in Earth's climate state include changes in ocean circulation due to the opening of Southern Ocean gateways (*4*), a decrease in atmospheric CO_2 (*5*–*8*), and a minimum in solar insolation (*2*).

How Earth's temperature changed during ice expansion is poorly defined, largely because benthic $\delta^{18}O$ records do not distinguish between ice volume and temperature. Deep-sea temperature records based on foraminiferal Mg/Ca ratios show little change during ice expansion (*9*–*11*). As a result, benthic $\delta^{18}O$ records imply E-O ice volumes that must be accommodated by Northern Hemisphere glaciation (*2*, *9*, *12*). This conclusion is nearly untenable given scant physical evidence for Northern Hemisphere ice sheets before the latest Miocene (*7*, *12*–*15*). Deep-water foraminiferal Mg/Ca ratios could be affected by factors other than temperature (*9*, *11*), including a deepening of the CCD (*2*) and changes in deep-water carbonate ion concentration that occurred during the E-O climate transition. Indeed, shallow-water Mg/Ca–based temperatures, from exceptionally well-preserved foraminifera deposited above the CCD, indicate ~2.5°C of cooling in the tropics (*14*, *15*) and cast further suspicion on deep-water Mg/Ca–based temperatures across this major CCD deepening event.

Here, we report E-O sea surface temperature (SST) changes, which were determined with alkenone unsaturation index ($U^{K'}_{37}$) and tetrather index (TEX_{86}) (*16*, *17*), from 11 globally dispersed ocean localities. These localities include Ocean Drilling Program/Deep Sea Drilling Project (ODP/DSDP) sites 277, 336, 511, 913, and 1090, with paleolatitudes between ~45° and 70° in both hemispheres (*18*), and sites 628, 803, 925, 929, 998, and 1218 in the tropics (Fig. 1 and table S1) (*19*). Chronologies for these sites were previously established or refined and/or determined in this study (table S2 and fig. S1). TEX_{86} indices were converted to SST by use of a modified temperature calibration based on all published ocean surface sediment data (fig. S2) (*20*). Nonetheless, older calibrations would yield qualitatively similar results over the temperature ranges observed.

Both $U^{K'}_{37}$ and TEX_{86} SSTs show substantial high-latitude cooling between ~34 and 33 Ma (Fig.

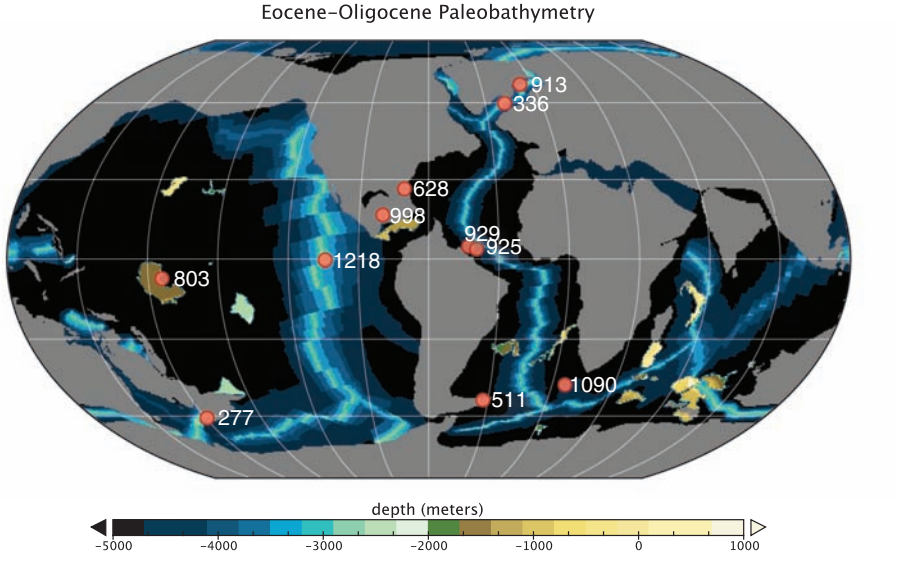

Fig. 1. Paleolocations of DSDP and ODP sites used in this study, superimposed on a map of reconstructed E-O bathymetry and geography (*18*).

[1]Department of Geology and Geophysics, Yale University, New Haven, CT 06520, USA. [2]Department of Earth Sciences, University of Hong Kong, Hong Kong, People's Republic of China. [3]Department of Geosciences, University of Massachusetts-Amherst, Amherst, MA 01003, USA. [4]Department of Earth and Atmospheric Sciences, Purdue University, West Lafayette, IN 47907, USA. [5]Laboratory of Palaeobotany and Palynology, Utrecht University, Budapestlaan 4, 3584 CD Utrecht, Netherlands. [6]Department of Earth and Planetary Sciences, Harvard University, Cambridge, MA 02138, USA.

*To whom correspondence should be addressed. E-mail: zhliu@hku.hk (Z.L.); mark.pagani@yale.edu (M.P.)

2). At sites 511 and 336, for which E-O transition records are relatively complete, SST cooled >5°C from the late Eocene to the early and mid-Oligocene, whereas maximum cooling at sites 277, 913, and 1090 occurred ~33.5 Ma. High-latitude cooling averaged ~4.8°C (using a direct average of all high-latitude data ranging from ~2° to ~8°C at individual sites) from the late Eocene (~34 to 37 Ma) to the earliest Oligocene (~33 to 34 Ma) (table S3 and fig. S4), or ~5.4°C at 33.4 Ma when determined by a 10-point running average of the combined high-latitude records (Fig. 2B). Our estimate of SST cooling is most likely a minimum value, given that the full magnitude of SST change is probably not expressed because of low resolution, core gaps, and sediment hiatuses close to the E-O boundary (fig. S4).

In general, the timing and pattern of high-latitude SST reconstructions from the late Eocene to early and mid-Oligocene correlate well with benthic $\delta^{18}O$ changes (Fig. 2) (*21*, *22*). SST reached the lowest values near the same time as the maximum $\delta^{18}O$ excursion at ~33.5 Ma, particularly at site 511 (Fig. 2C). Given the resolution of our entire data set, high-latitude SST changes appear to be approximately synchronous with benthic $\delta^{18}O$ changes during the climate transition.

Our records also indicate that late Eocene high-latitude SST was substantially warmer than previous estimates. Before the E-O climate transition (~34 to 37 Ma), high-latitude SST was ~20°C [±2.7°C for $U^{K'}_{37}$ and ±3.7°C for TEX_{86} (*19*)] (Fig. 2A), which is ~10°C warmer than temperatures derived from benthic and planktonic $\delta^{18}O$ records from deep-sea cores (*21*, *23*). Some localities, such as site 277, exhibit extraordinarily warm SST, with temperatures reaching ~27°C. Differences between our records and benthic/planktonic $\delta^{18}O$ records could be explained in various ways: diagenesis, seasonality, and/or locations of deep-water production. Diagenesis could potentially alter both $U^{K'}_{37}$ (*24*) and TEX_{86} (*25*) indices, resulting in temperature estimates warmer than original SSTs. However, there is no consistently strong evidence that $U^{K'}_{37}$ (*24*) or TEX_{86} (*26*) values are radically altered by diagenesis. In addition, diagenetic pathways differ for these two distinct proxies, yet SST estimates yield remarkably similar results (Fig. 2A). Two relatively complete records from sites 511 and 336 indicate that the coldest early Oligocene $U^{K'}_{37}$ SST was only ~3° to 6°C warmer when compared with the same locations today (table S1). Although these warmer-than-modern temperatures are anticipated for the early Oligocene, they also constrain warm-temperature biases introduced by diagenetic effects for Oligocene and late Eocene to smaller than 3° to 6°C. Finally, our late Eocene proxy records from the high latitudes are broadly consistent with other documented marine and terrestrial biotic changes (*27*, *28*) and terrestrial temperature records (*29*, *30*).

Discrepancies between foraminiferal $\delta^{18}O$– and organic-based temperature estimates could also reflect differences in the locations of our sites relative to deep-water sources as well as the seasonality of foraminifera versus organic production. Paired benthic and planktonic $\delta^{18}O$ records during this time show systematic offsets to at least 65°S, and SST gradients of 7° to 10°C between mid- to high-latitude sites such as 511 and 1090, and polar site 690 (*23*), indicating that deep-water formation was probably focused across latitudes higher than those represented by our site localities. Further, benthic $\delta^{18}O$ values reflect deep-water production during winter months, whereas $U^{K'}_{37}$ and TEX_{86} values capture mean annual SSTs that were probably biased toward late spring/early autumn temperatures near the poles. Our model results also

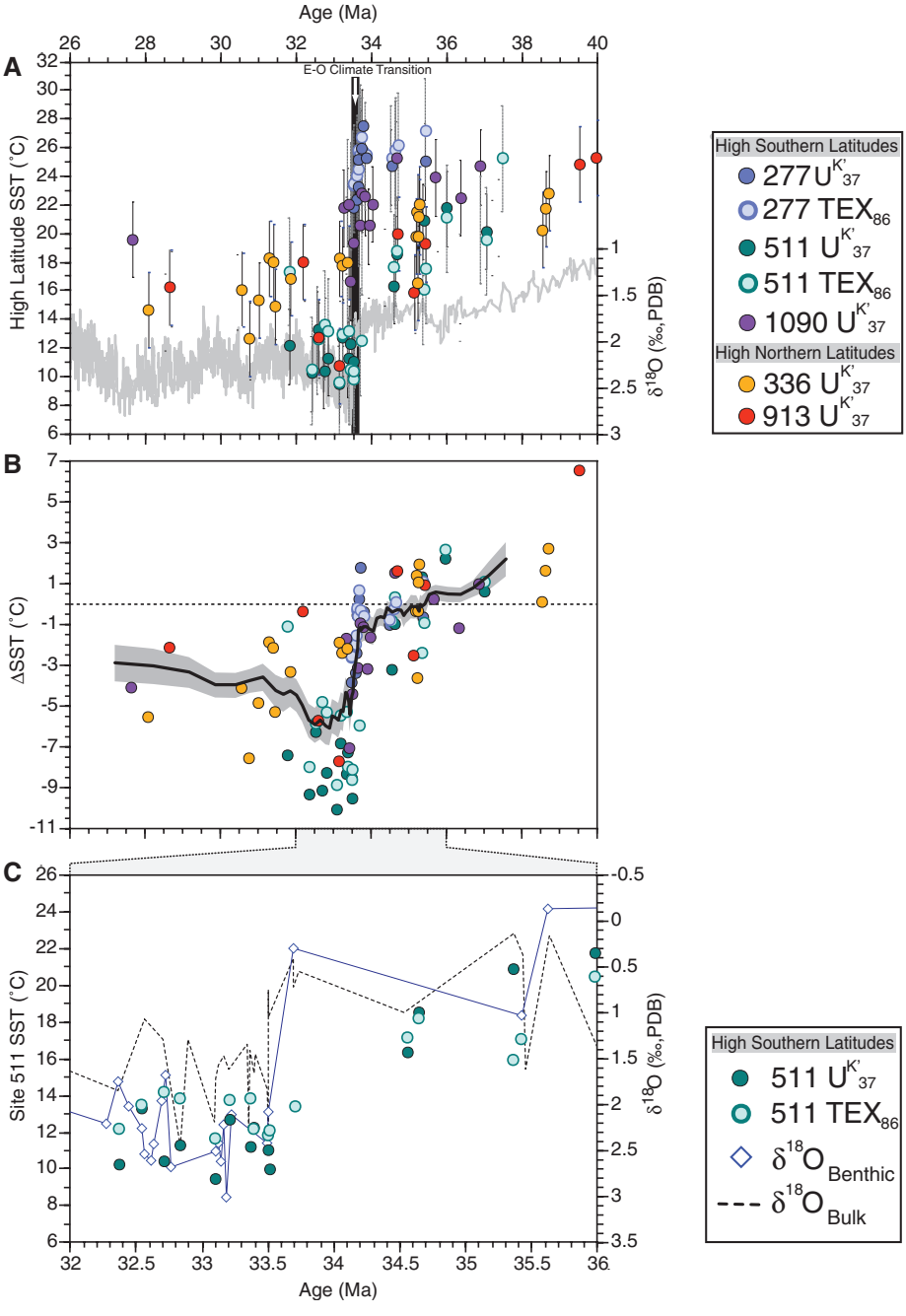

Fig. 2. High-latitude SST records during the late E-O. (**A**) SST reconstructions from five high-latitude sites. The gray line represents a composite benthic $\delta^{18}O$ record (*21*). SST calibration equations for $U^{K'}_{37}$ and TEX_{86} are SST = $(U^{K'}_{37} - 0.039)/0.034$ (*16*) and SST = $50.47 - 16.33/TEX_{86}$, respectively (*19*). SST uncertainty is based on 1σ SE of their respective calibration regressions (fig. S3). (**B**) Changes in SST represented as temperature deviations from mean values at each site before the E-O transition (~34 to 37 Ma). The solid black line represents a 10-point running average of SST changes from all high-latitude sites and yields ~5.4°C of cooling at 33.4 Ma. The shaded region brackets the SE of the 10-point running average. The dotted line marks zero SST change relative to the pre–E-O (~34 to 37 Ma) SST average. (**C**) A detailed comparison of $U^{K'}_{37}$ and TEX_{86} SST values with $\delta^{18}O$ records of benthic foraminifera (*22*) and bulk carbonate during the E-O transition at site 511.

show that it is possible to sustain ~20°C annual mean temperatures in mid- to high-latitude regions, with near-freezing winter temperatures in the polar coastal waters that reflect deep-water formation regions (fig. S5). Recent evidence suggests that Mg/Ca and $\delta^{18}O$ SST estimates from well-preserved early and late Eocene planktonic foraminifera are broadly consistent with TEX_{86} estimates but ~10°C warmer than other $\delta^{18}O$ estimates from the tropics (*14*, *31*) and high latitudes (*32*), suggesting that the primary planktonic $\delta^{18}O$ values (*23*) were altered by early diagenesis (*31*). Although our late Eocene SST estimates from site 277 and probably site 1090 (Fig. 2A) appear particularly warm when compared with other high-latitude sites investigated here, they are in accord with early and mid-Eocene SST estimates from New Zealand, based on the TEX_{86} proxy, Mg/Ca, and $\delta^{18}O$ values from extraordinarily well-preserved planktonic foraminifera (*32*). Thus, we suggest that our high-latitude estimates, because of biases introduced by diagenesis and seasonal production, are probably at the warm end of but remain close to the E-O mean annual temperatures. Physical interpretation of exceptional high-latitude warmth during the late Eocene remains an important challenge to climate scientists.

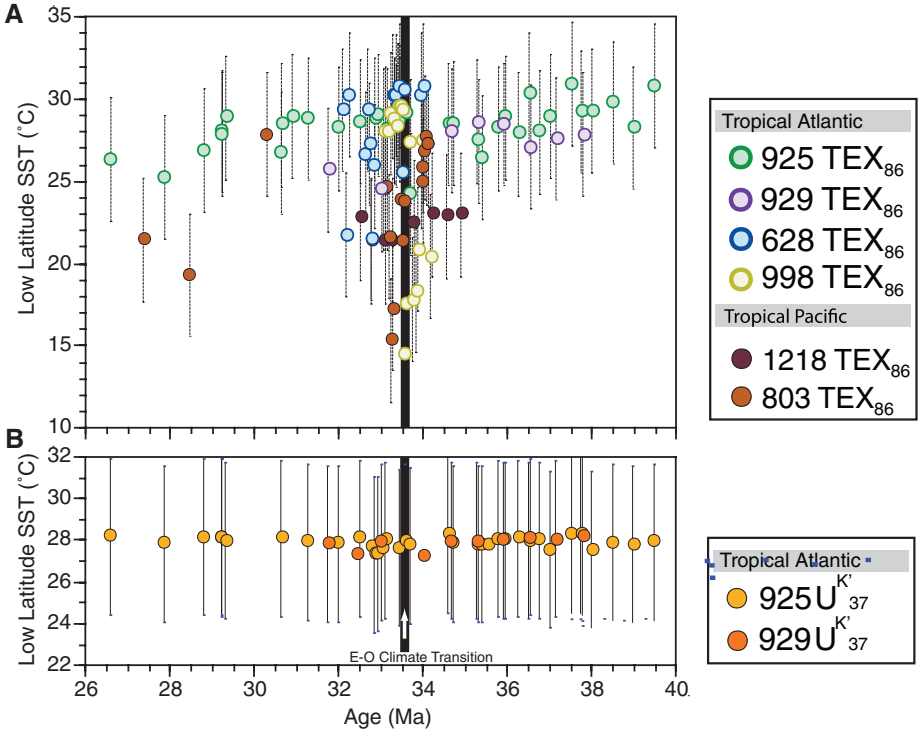

Fig. 3. Tropical SST records during the late E-O. (**A**) TEX_{86} SST records from six tropical sites. (**B**) $U^{K'}_{37}$-SST records from sites 925 and 929. The TEX_{86} proxy probably overestimates the magnitude of tropical SST changes because of tropical oceanographic perturbations associated with high-latitude cooling.

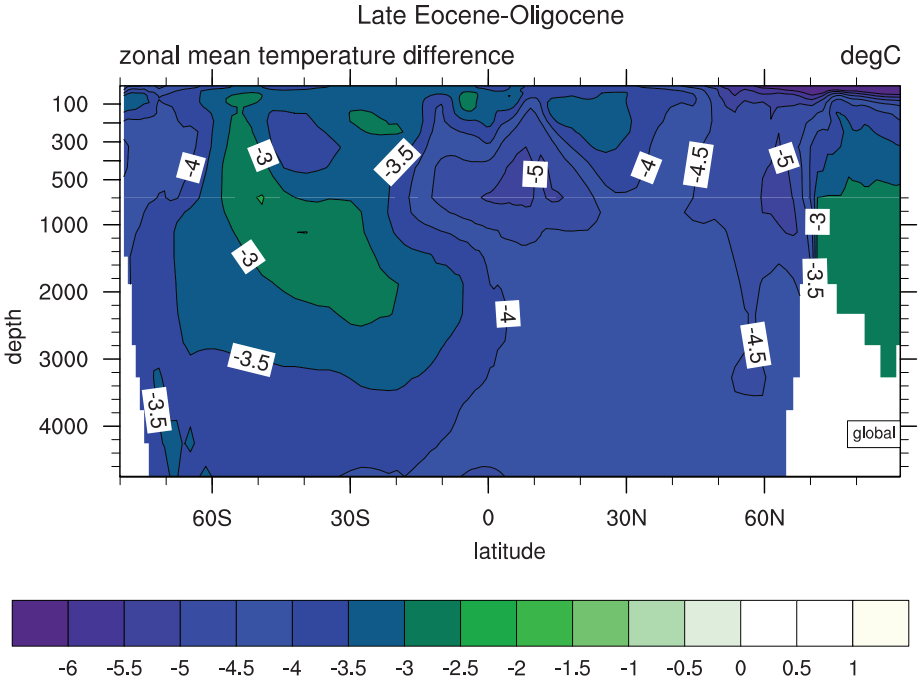

Fig. 4. Fully coupled E-O model results. The zonally and annually averaged temperature difference between the high and low partial pressure of CO_2 cases described in (*19*), representing late Eocene and early Oligocene conditions, is shown. Cooling is maximized in the equatorial upper thermocline below the mixed-layer, high-latitude oceans in the upper 2 km and in the abyss, predominately north of the equator. The vertical scale (in meters) is stretched.

Compared with high-latitude E-O SST, tropical TEX_{86}-SST records are more difficult to interpret. Tropical SST predominantly range between 27° to 31°C before ~34 Ma and after ~32 Ma. A brief interval (between ~33 to 34 Ma) of apparent colder temperatures is expressed in most of our tropical TEX_{86}-SST records, with inferred temperature changes varying from 0° to 15°C (Fig. 3A). However, such large tropical SST variations require physically improbable atmospheric and oceanic circulations when considered within the context of spatial temperature gradients that drive wind fields (*8*). Further, large tropical SST changes are unsupported by other tropical Mg/Ca-based SST reconstructions from well-preserved foraminifera (*14*, *15*). Indeed, $U^{K'}_{37}$ values from sites 925 and 929 in the tropical Atlantic indicate temperatures >27°C and do not support the large temperature variability suggested by some of our TEX_{86} records (Fig. 3B). Given these considerations, we suggest that large tropical TEX_{86} perturbations do not solely record SST variations. Instead, extreme TEX_{86} values probably reflect changes in tropical water-column properties, associated with high-latitude surface cooling identified here, and variations in the population and production depths of Crenarchaeota (*20*, *33*). If we consider only TEX_{86} records with temperature variations constrained by coeval $U^{K'}_{37}$ records (sites 925 and 929), tropical cooling does not appear to exceed ~3°C (table S3), which is consistent with other tropical temperature records (*14*, *15*).

Our results affect interpretations of ice volume and the potential for Northern Hemisphere glaciation during the E-O climate transition. Ice-volume calculations, based on benthic $\delta^{18}O$ records, require an estimate of deep-ocean cooling. However, the full change in SST from sparsely sampled localities is not necessarily translated to abyssal depths. To evaluate how surface temperature change was translated into the deep ocean, we ran coupled atmosphere-ocean simulations with Eocene boundary conditions (*8*) and CO_2 levels representative of pre- and posttransition atmospheric mixing ratios (*5*, *6*) (*19*). Model simulations reproduce ~5°C of

high-latitude cooling consistent with our data, a 3.8°C volumetric-mean ocean cooling, and global-mean surface cooling of 4.4°C (Fig. 4). The model provides clear evidence of spatially heterogenous benthic cooling, averaging ~4°C (that is, somewhat less than the surface temperature change). However, because (i) these model simulations do not account for temperature feedbacks related to growing ice sheets and (ii) our estimate of ~5°C of high-latitude cooling might represent a minimum value, model results for deep-water temperature change also potentially slightly underestimate the magnitude of cooling. Therefore, the combination of our model and proxy results provides a range between 3° and 5°C of benthic cooling during the E-O climate transition, with our best estimate converging on 4°C.

Assuming that the average $\delta^{18}O$ value of Oligocene Antarctic ice sheets was ~20 ‰ more positive relative to today (an assumption that maximizes ice-volume estimates) (*34*), the growth of continental ice implied by a +1.5 ‰ shift in benthic $\delta^{18}O$ and a benthic cooling of 3° to 5°C is between ~10×10^6 and 30×10^6 km^3. This estimate is equivalent to ~50 to 140% of the volume of a simulated early Oligocene East Antarctic ice sheet (*5*, *34*) or ~40 to 120% of modern Antarctic ice volume and 30 to 100% of Antarctic ice volume during the Last Glacial Maximum. Although our results do not contradict evidence of small localized glaciers in the northern high latitudes (*13*), estimated ice volumes could be easily accommodated on Antarctica alone (*34*) and do not require Northern Hemisphere glaciation (*12*) to explain the magnitude of the benthic $\delta^{18}O$ shift. Finally, between ~33 and 34 Ma, our data support a pattern of systematic cooling in both the northern and southern high latitudes (Fig. 2A) that was approximately in phase with benthic $\delta^{18}O$ changes (Fig. 2C)—a temporal pattern also observed in other tropical records (*14*, *15*). These results are consistent with a scenario of global cooling forced by a reduction in greenhouse gas concentration rather than the more regionalized effects of ocean gateways (*5*–*8*).

References and Notes

1. K. G. Miller, R. G. Fairbanks, G. S. Mountain, *Paleoceanography* **2**, 1 (1987).
2. H. K. Coxall, P. A. Wilson, H. Palike, C. H. Lear, J. Backman, *Nature* **433**, 53 (2005).
3. N. J. Shackleton, J. P. Kennett, *Initial Rep. Deep Sea Drill. Proj.* **29**, 743 (1975).
4. J. P. Kennett, *J. Geophys. Res.* **82**, 3843 (1977).
5. R. M. DeConto, D. Pollard, *Nature* **421**, 245 (2003).
6. M. Pagani, J. C. Zachos, K. H. Freeman, B. Tipple, S. Bohaty, *Science* **309**, 600 (2005).
7. R. DeConto, D. Pollard, D. Harwood, *Paleoceanography* **22**, Pa3214 (2007).
8. M. Huber, D. Nof, *Palaeogeogr. Palaeoclimatol. Palaeoecol.* **231**, 9 (2006).
9. C. H. Lear, Y. Rosenthal, H. K. Coxall, P. A. Wilson, *Paleoceanography* **19**, Pa4015 (2004).
10. C. H. Lear, H. Elderfield, P. A. Wilson, *Science* **287**, 269 (2000).
11. K. Billups, D. P. Schrag, *Earth Planet. Sci. Lett.* **209**, 181 (2003).
12. A. K. Tripati *et al.*, *Earth Planet. Sci. Lett.* **265**, 112 (2008).
13. J. S. Eldrett, I. C. Harding, P. A. Wilson, E. Butler, A. P. Roberts, *Nature* **446**, 176 (2007).
14. C. H. Lear, T. R. Bailey, P. N. Pearson, H. K. Coxall, Y. Rosenthal, *Geology* **36**, 251 (2008).
15. M. E. Katz *et al.*, *Nat. Geosci.* **1**, 329 (2008).
16. F. G. Prahl, L. A. Muehlhausen, D. L. Zahnle, *Geochim. Cosmochim. Acta* **52**, 2303 (1988).
17. S. Schouten, E. C. Hopmans, E. Schefuss, J. S. Sinninghe Damsté, *Earth Planet. Sci. Lett.* **204**, 265 (2002).
18. R. D. Müller, M. Sdrolias, C. Gaina, B. Steinberger, C. Heine, *Science* **319**, 1357 (2008).
19. Materials and methods are available as supporting material on *Science* Online.
20. J.-H. Kim, S. Schouten, E. C. Hopmans, B. Donner, J. S. Sinninghe Damsté, *Geochim. Cosmochim. Acta* **72**, 1154 (2008).
21. J. Zachos, M. Pagani, L. Sloan, E. Thomas, K. Billups, *Science* **292**, 686 (2001).
22. J. P. Muza, D. F. Williams, S. W. Wise, *Initial Rep. Deep Sea Drill. Proj.* **71**, 409 (1983).
23. J. C. Zachos, L. D. Stott, K. C. Lohmann, *Paleoceanography* **9**, 353 (1994).
24. J. O. Grimalt *et al.*, *Geochem. Geophys. Geosys.* **1**, 2000GC000053 (2000).
25. S. R. Shah, G. Mollenhauer, N. Ohkouchi, T. I. Eglinton, A. Pearson, *Geochim. Cosmochim. Acta* **72**, 4577 (2008).
26. S. Schouten, E. C. Hopmans, J. S. Sinninghe Damsté, *Org. Geochem.* **35**, 567 (2004).
27. H. Brinkhuis, H. Visscher, *Soc. Econ. Paleontol. Mineral. Spec. Publ.* **54**, 295 (1995).
28. D. R. Prothero, T. H. Heaton, *Palaeogeogr. Palaeoclimatol. Palaeoecol.* **127**, 257 (1996).
29. S. Schouten *et al.*, *Geology* **36**, 147 (2008).
30. A. Zanazzi, M. J. Kohn, B. J. MacFadden, D. O. Terry, *Nature* **445**, 639 (2007).
31. P. N. Pearson *et al.*, *Geology* **35**, 211 (2007).
32. C. J. Hollis *et al.*, *Geology* **37**, 99 (2009).
33. C. Turich *et al.*, *Geochim. Cosmochim. Acta* **71**, 3272 (2007).
34. R. M. DeConto *et al.*, *Nature* **455**, 652 (2008).

35. The authors thank S. Schouten and E. Hopmans for their assistance in establishing an interlaboratory calibration, J. Eldrett for advice on the site 913 age model, M. Woodruff of the University of Massachussetts Stable Isotope Facility for analyses of site 511 material, and Integrated Ocean Drilling Program for providing samples. The reviews of P. Wilson and one anonymous referee greatly improved the manuscript. This work was supported by a postdoctoral fellowship provided by Yale University and a Major Research Instrumentation grant from NSF. Computing was performed on Rosen Center for Advanced Computing resources within Information Technology at Purdue. M.H.'s contribution is partially supported by the New Zealand's Global Change Through Time Programme at GNS Science.

Supporting Online Material

www.sciencemag.org/cgi/content/full/323/5918/1187/DC1
Materials and Methods
Figs. S1 to S5
Tables S1 to S3
References

24 September 2008; accepted 23 January 2009
10.1126/science.1166368

Seeing the Fermi Surface in Real Space by Nanoscale Electron Focusing

Alexander Weismann,[1,2] Martin Wenderoth,[1]* Samir Lounis,[3] Peter Zahn,[4] Norbert Quaas,[1] Rainer G. Ulbrich,[1] Peter H. Dederichs,[3] Stefan Blügel[3]

The Fermi surface that characterizes the electronic band structure of crystalline solids can be difficult to image experimentally in a way that reveals local variations. We show that Fermi surfaces can be imaged in real space with a low-temperature scanning tunneling microscope when subsurface point scatterers are present: in this case, cobalt impurities under a copper surface. Even the very simple Fermi surface of copper causes strongly anisotropic propagation characteristics of bulk electrons that are confined in beamlike paths on the nanoscale. The induced charge density oscillations on the nearby surface can be used for mapping buried defects and interfaces and some of their properties.

The coherent propagation of electrons in solids is central for a variety of phenomena that are at the core of modern physics. Scanning tunneling microscopy (STM) has been used to manipulate atoms and create structures that allow standing electron wave patterns to be visualized (*1*). C. R. Moon *et al.* (*2*) extended this line of investigations to the retrieval of quantum-phase information in nanostructures with the scanning tunneling microscope. Another facet of electron propagation has been revealed by measurements (*3*) of exchange interaction between adatoms and wires mediated through the Ruderman-Kittel-Kasuya-Yosida (RKKY) mechanism (*4*) on a platinum surface. All of these effects depend on a fundamental property of the electron sea: It rearranges itself to minimize the disturbance caused by foreign atoms. These Friedel oscillations (*5*) may cause technologically important effects such as the formation of diluted magnetic semiconductors, spin-glasses, or the interlayer exchange coupling between magnetic layers (*6*) exploited in read heads of magnetic hard discs.

[1]IV Physikalisches Institut, Universität Göttingen, 37077 Göttingen, Germany. [2]Courant Research Center Göttingen, 37077 Göttingen, Germany. [3]Institut für Festkörperforschung and Institut for Advanced Simulation, Forschungszentrum Jülich, 52425 Jülich, Germany. [4]Fachbereich Physik, Martin-Luther-Universität Halle-Wittenberg, 06099 Halle, Germany.

*To whom correspondence should be addressed. E-mail: wenderoth@ph4.physik.uni-goettingen.de